THE JOURNAL OF PHYSICAL CHEMISTRY C

Article

pubs.acs.org/JPCC

Investigating Li_2NiO_2–Li_2CuO_2 Solid Solutions as High-Capacity Cathode Materials for Li-Ion Batteries

Jing Xu,[†] Sara Renfrew,[§] Matthew A. Marcus,[‡] Meiling Sun,[†] Bryan D. McCloskey,[†,§] and Wei Tong*[,†]

[†]Energy Storage and Distributed Resources Division and [‡]Advanced Light Source, Lawrence Berkeley National Laboratory, Berkeley, California 94720 United States

[§]Department of Chemical and Biomolecular Engineering, University of California, Berkeley, California 94720, United States

Supporting Information

ABSTRACT: $Li_2Ni_{1-x}Cu_xO_2$ solid solutions were prepared by a solid-state method to study the correlation between composition and electrochemical performance. Cu incorporation improved the phase purity of $Li_2Ni_{1-x}Cu_xO_2$ with orthorhombic *Immm* structure, resulting in enhanced capacity. However, the electrochemical profiles suggested Cu incorporation did not prevent irreversible phase transformation during the electrochemical process, instead, it likely influenced the phase transformation upon lithium removal. By combining ex situ X-ray diffraction (XRD), X-ray absorption spectroscopy (XAS), and differential electrochemical mass spectrometry (DEMS) measurements, this study elucidates the relevant phase transformation (e.g., crystal structure, local environment, and charge compensation) and participation of electrons from lattice oxygen during the first cycle in these complex oxides.

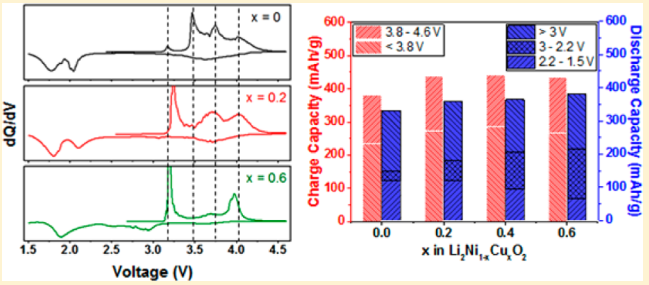

INTRODUCTION

Li-ion batteries have been extensively used in portable electronics and are now being pushed toward transportation and grid applications.[1,2] To catch up with the pressing demand for economically accessible and environmentally benign energy storage devices, new research strategies based on chemistry that can accommodate two electron transport processes have been proposed for the search of new electrode materials with even higher energy density.[3−5] Among all the candidates, Li_2NiO_2 has gained research interest for possible use as Li-ion cathodes because it potentially allows the utilization of the Ni^{2+}/Ni^{4+} redox couple with two Li per formula unit, resulting in a theoretical capacity of 513 mAh/g.[6−10] Li_2NiO_2 was first prepared for use in Li-ion batteries by Dahn et al. through the intercalation of one additional Li into layered $LiNiO_2$.[6] Li_2NiO_2 formed via the electrochemical lithiation process is isostructural with $Ni(OH)_2$ and can be indexed in the $P\bar{3}m1$ space group. The crystal structure is composed of layers of octahedral Ni and tetrahedral Li that are alternatively arranged between close-packed oxygen layers.[11] However, the ground state of Li_2NiO_2 is not $P\bar{3}m1$ structure, but an orthorhombic form with *Immm* space group, in which Ni sits on the square planar site and Li occupies the tetrahedral site.[7,12] Kang et al. reported the synthesis and electrochemistry of an orthorhombic Li_2NiO_2, which exhibited a charge capacity of ∼320 mAh/g and a discharge capacity of about 240 mAh/g between 1.5 and 4.6 V. However, the *Immm* structure was not robust, which transformed to an amorphous layered structure along with NiO after cycling.[7] This structural instability poses a serious challenge for use in rechargeable Li-ion batteries, although reasonably fast Li motion along the *b* axis and the diagonal direction between *a* and *b* axes was predicted for this material.[13]

Li_2CuO_2 is isostructural with Li_2NiO_2 and also belongs to the orthorhombic *Immm* space group. Its electrochemical delithiation process involves three types of phases: $Li_{1+y}CuO_2$, $Li_{1.5}CuO_2$, and $Li_{2-z}CuO_2$ ($0.5 \leq y, z \leq 1$)),[14,15] where $LiCuO_2$ and $Li_{1.5}CuO_2$ crystallize in the monoclinic $C2/m$ space group.[15−17] The crystal lattice of all three compounds contains a CuO_4 square unit, which shares edges with tetrahedral LiO_4 in Li_2CuO_2, one tetrahedral LiO_4 and one octahedral LiO_6 in $Li_{1.5}CuO_2$, and only octahedral LiO_6 in $LiCuO_2$, therefore, its delithiation process is mainly characterized by a gradual change in Li environment from tetrahedral to octahedral coordination.[14] Earlier attempts were made to prepare Li_2NiO_2–Li_2CuO_2 solid solutions[18−21] for Li-ion battery application because of the similar square planar coordination[15−17,22−25] and promising electrochemical features.[14,26−33] The intermediate composition, $Li_2Cu_{0.5}Ni_{0.5}O_2$, demonstrated a balance between capacity and reversibility compared to the end members, Li_2NiO_2 and Li_2CuO_2.[18] Recently, Ruther et al. performed a comprehensive study on the electrochemical reaction mechanism of $Li_2Cu_{0.5}Ni_{0.5}O_2$ using a suite of characterization techniques, revealing a reversible Ni^{2+}/Ni^{3+} redox reaction coupled with O_2 evolution at a high charge voltage (>3.9 V) and Cu^{2+} to Cu^+ reduction at a low discharge voltage (<1.8 V).[21] Oxygen oxidation was also proposed and

Received: February 23, 2017
Revised: May 4, 2017
Published: May 11, 2017

DOI: 10.1021/acs.jpcc.7b01799
J. Phys. Chem. C 2017, 121, 11100−11107

gas evolution was detected by other groups,[25,31] but no quantification work has been performed to isolate the evolved gas species and correlate the oxygen redox with electrochemistry.

In our work, $Li_2Ni_{1-x}Cu_xO_2$ solid solutions were synthesized in order to study the effect of Cu incorporation on the overall electrochemical behavior. Because the phase transformation presents a critical concern for this family of materials, the crystal structure, local environment, as well as the charge compensation during the first cycle were studied by a combination of X-ray diffraction (XRD), X-ray absorption spectrometry (XAS), and differential electrochemical mass spectroscopy (DEMS). This in-depth understanding of the phase and electrochemical behavior will provide useful guidance for the further development of these high-capacity materials.

EXPERIMENTAL SECTION

Material Synthesis. Li_2O (Alfa Aesar), NiO (Alfa Aesar), and CuO (Alfa Aesar) precursors were used to synthesize $(1-x)Li_2NiO_2{\cdot}xLi_2CuO_2$ solid solutions. Precursors with designated Ni and Cu ratios were loaded into a stainless steel jar in Ar-filled glovebox and milled on Spex 8000 for 3 h. Then the milled powder was annealed at 700 °C for 12 h with continuous N_2 flow.

Electrochemical Characterization. $Li_2Ni_{1-x}Cu_xO_2$ electrodes are composed of 80 wt % active material, 15 wt % carbon black as conductive agent, and 5 wt % polyethylenetetrafluoride (PTFE) as binder. 2032-Type coin cells were assembled in an Ar-filled glovebox (H_2O < 0.1 ppm) with Li metal as the negative electrode. A Celgard 2400 separator and 1 M $LiPF_6$ electrolyte solutions in 1:2 w/w ethylene carbonate−diethyl carbonate (Ferro Corporation) solvent were used to fabricate the cells. Galvanostatic discharge and charge were performed on a Maccor 4200 battery cycler between 4.6 and 1.5 V at a current density of 12 mA/g.

Physical Characterization. X-ray diffraction patterns were collected using a Bruker D2-Phaser with Cu Kα radiation (λ = 1.54178 Å). Hard X-ray absorption spectra were collected in transmission mode using a (220) monochromator at SSRL beamline 4-1. Higher harmonics in the X-ray beam were reduced by detuning the Si (220) monochromator. Energy calibration was accomplished by using the first inflection points in the spectra of Ni foil reference. XANES data were analyzed by Sam's Interface for XAS Package or SIXPACK software, with the Photoelectron Energy Origin E_0 determined by the first inflection point of the absorption edge jump. All ex situ measurements were carefully handled by sealing the samples with Kapton films inside an Ar-filled glovebox to ensure a good protection and avoid the air/moisture exposure. DEMS measurements were taken on a customized Swagelok type cell that was connected to a high-pressure gas chromatography (HPGC) valve, the details of DEMS setup and measuring protocol were described in a previous publication.[34] Typical error of this DEMS measurement is about 3%. The DEMS cell was charged after an initial rest at open circuit voltage for 6 h and charge/discharge was done under potentiostatic control using a BioLogic SP-300 potentiostat.

RESULTS AND DISCUSSION

X-ray Diffraction (XRD). All the samples were synthesized via a solid-state method by high-energy milling the mixture of Li_2O, NiO, and CuO precursors for 3 h, then annealing at 700 °C for 12 h under N_2 atmosphere. Figure 1 shows the XRD patterns of the four samples with Ni content $(1-x)$ ranging

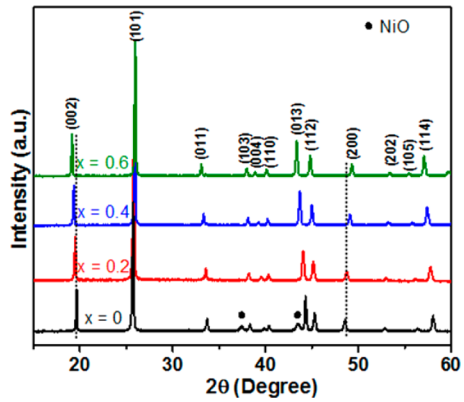

Figure 1. X-ray diffraction patterns of $Li_2Ni_{1-x}Cu_xO_2$ (x = 0, 0.2, 0.4, 0.6).

from 1 to 0.4. Overall, all the major XRD peaks in these samples could be indexed as the *Immm* space group. Close examination of the XRD patterns revealed a small amount of NiO impurity in the final product of Li_2NiO_2, whereas, the Cu substitution removed the NiO impurity and facilitated the formation of pure *Immm*-type phase. In addition, shifts of the XRD diffraction peaks were observed with increasing Cu content, for example, the (002) and (200) peaks that are labeled by dash lines. Such peak shifting resulted from the substitution of a larger Cu ion on the Ni site, suggesting the formation of a solid solution between isostructural Li_2NiO_2 and Li_2CuO_2.

Electrochemistry. The first cycle voltage profiles are displayed in Figure 2a. Li_2NiO_2 delivered a capacity of 380 mAh/g during the first charge and 330 mAh/g during the first discharge. With Cu substituted, both charge and discharge capacities increased; the total charge capacity increased up to ~440 mAh/g at 0.2 Cu and showed little change with Cu content. Such increase in charge capacity mainly occurred at <3.8 V (Figure 2b), presumably ascribed to the removal of electrochemically inactive NiO impurity in the Cu substituted samples. On the other hand, the Cu substitution resulted in a substantial change in the charge profiles, which progressively decomposed into two distinguishable plateau regions around 3.2 and 3.6 V. They became more pronounced in the differential capacity curves (Figure 2c). The dQ/dV of Li_2NiO_2 during the charge showed several small oxidation peaks around 3.2, 3.5, 3.7, and 4.0 V. Based on first-principles calculations, the first three could be possibly associated with the phase transformation from *Immm* Li_2NiO_2 to $R\bar{3}m$ and *Immm* $LiNiO_2$, and $R\bar{3}m$ NiO_2. However, the difficulty in differentiating $R\bar{3}m$ and *Immm* type $LiNiO_2$ phase is noted because the small voltage difference (~0.2 V) fell within the uncertainty of calculations.[7] With 0.2 Cu substitution, oxidation peaks around 3.7 and 4.0 V remained as the main features, but the oxidation peak around 3.2 V appeared to grow at the expense of the peak at 3.5 V. Further increasing Cu content to 0.6, only sharp oxidation peaks at 3.2 and 4.0 V were observed, which was consistent with that of charged Li_2CuO_2.[25] Clearly, we can conclude that the phase transition at 3.2 V was promoted by Cu substitution,[14] and the peak at 4.0 V was a common feature of the Li_2NiO_2 and Li_2CuO_2 charging process.

DOI: 10.1021/acs.jpcc.7b01799
J. Phys. Chem. C 2017, 121, 11100−11107

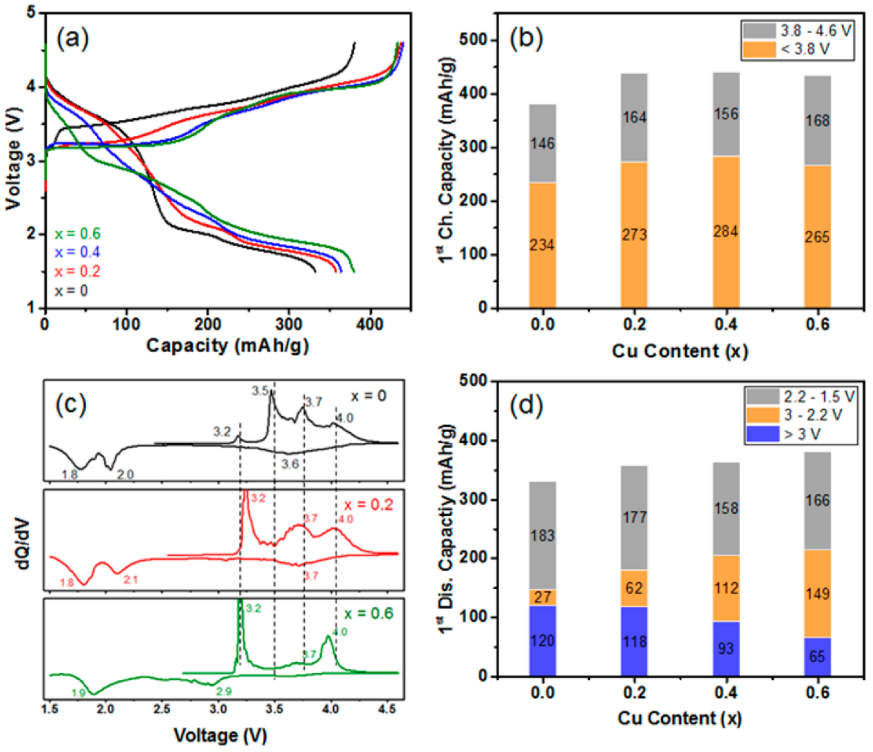

Figure 2. (a) Voltage profiles, (b) charge capacity distribution, (c) selected dQ/dV plots, and (d) discharge capacity distribution of $Li_2Ni_{1-x}Cu_xO_2$ (x = 0, 0.2, 0.4, 0.6) during the first cycle. Cells were cycled at 12 mA/g between 4.6 and 1.5 V.

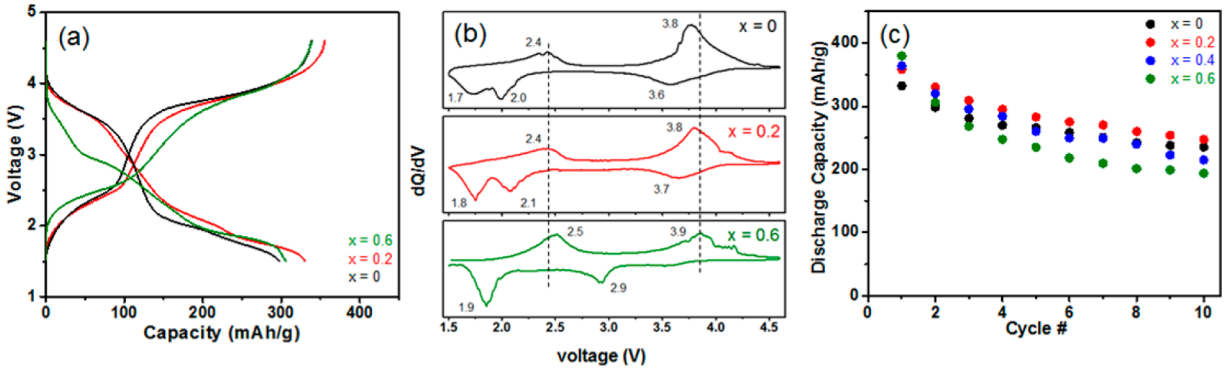

Figure 3. Selected second cycle (a) voltage profiles and (b) dQ/dV plots, and (c) cycling performance of $Li_2Ni_{1-x}Cu_xO_2$ (x = 0, 0.2, 0.4, 0.6). Cells were cycled at 12 mA/g between 4.6 and 1.5 V.

Meanwhile, the discharge capacity increased with Cu content and reached 380 mAh/g at 0.6 Cu. The discharge profile of Li_2NiO_2 was characterized by three reduction peaks around 3.6, 2.0, and 1.8 V. The absence of additional reduction peaks in the high voltage region (>3 V) was an evidence of the irreversible phase transformation. With Cu substitution, the change in the discharge profile was significant. We can clearly see the shift of the discharge voltage profile from >3 V toward a lower voltage region (3−2.2 V). With increasing Cu content to 0.6, the plateaus at 3.6 and 2.0 V gradually diminished and a new plateau around 2.9 V was observed, which seems to indicate a Cu-dominated phase transformation.[14] If we roughly divided the whole discharge profiles into three regions, the variation in discharge capacity in different voltage regions became more pronounced (Figure 2d). A clear trend in capacity vs Cu content was observed, being represented by a decrease at >3 V and an increase between 3 and 2.2 V.

The effect of Cu substitution on the voltage profiles was further examined in the subsequent cycle. The selected second cycle voltage profiles and dQ/dV plots are shown in Figure 3a,b. In general, a capacity loss was observed in both charge and discharge compared to the first cycle. Additionally, the irreversible and drastic structural change after the first cycle led to the amorphous electrodes. When we compared the features in dQ/dV plots, the most distinct difference between the first and second charge were the removal of the oxidation peaks around 3.2, 3.5, and 4.0 V and a newly developed oxidation peak around 2.4 V during the second charge. The second charge dQ/dV plot that was characterized by two broad oxidation peaks around 3.8 and 2.4 V showed consistency with those of layered $LiNiO_2$, corresponding to Ni^{3+}/Ni^{4+} redox between $LiNiO_2$ and $Li_{1-x}NiO_2$ and Ni^{2+}/Ni^{3+} redox between $Li_{1+y}NiO_2$ and $LiNiO_2$, respectively.[6] The rest features in the second discharge dQ/dV plot appeared almost no change compared to those in the first discharge. Such distinct features

DOI: 10.1021/acs.jpcc.7b01799
J. Phys. Chem. C 2017, 121, 11100−11107

suggested, after the first charge, the electrodes experienced an irreversible phase transformation, which constantly remained in the subsequent cycles. As such, the cycling performance of these four samples is presented in Figure 3c. Although the Cu substitution improved the discharge capacity in the initial cycle, the capacity retention was not effectively enhanced within the tested voltage window (4.6−1.5 V). Of all the four materials, an intermediate composition, $Li_2Ni_{0.8}Cu_{0.2}O_2$, was chosen for further studies on the electrochemical mechanism considering a substantial change in the first charge profile, preserved features during the discharge, and relatively good capacity and retention.

Ex Situ X-ray Diffraction (Ex Situ XRD). To elucidate the structural evolution, ex situ XRD was collected at various states of charge during the first cycle. The ex situ XRD patterns were immediately collected on the cycled $Li_2Ni_{0.8}Cu_{0.2}O_2$ electrodes by disassembling the cells once the designated voltages were reached. As shown in Figure 4a,b, a new set of diffraction peaks

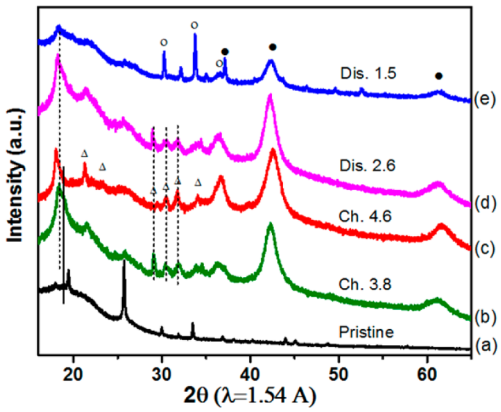

Figure 4. Ex situ XRD patterns of $Li_2Ni_{0.8}Cu_{0.2}O_2$ electrodes at (a) pristine state, (b) 3.8 V charge, (c) 4.6 V charge, (d) 2.6 V discharge, and (e) 1.5 V discharge. Li_2O, Li_2CO_3, and NiO are indicated by open circles, open triangles, and solid circles, respectively.

represented by the dash lines developed after charging the electrode to 3.8 V. The accurate assignment of these peaks is challenging due to the lack of long-range crystalline order. Combination of careful searching/matching in ICDD Powder Diffraction Database and potential phase development during the charge process led to a match of several possible phases. First of all, the XRD peaks (marked by dash lines) showed possible consistency with monoclinic $Li_{1+\delta}CuO_2$ ($0 \le \delta \le 0.5$) in $C2/m$ space group. Comparison of the XRD patterns at charged states to those of reference compounds are given in Figure S1. Variation in the XRD peak position and intensity between 29 and 35° might correlate with the size difference between nickel and copper ions and lithium content.[20,27] On the other hand, the distinct diffraction peak around 18.5° overlaps with (003) peak of layered $R\bar{3}m$ $LiNiO_2$[9,20] and Li_2CO_3 marked by open triangles certainly contributes to the weak peaks in the range of 29−35°. It should be pointed out that the coordination of Ni and Cu in layered $R\bar{3}m$ $LiNiO_2$ and $C2/m$ $Li_{1+\delta}CuO_2$ is different, being represented by $[NiO_6]$ vs $[CuO_4]$. Combined with our hard XAS results, we are certain about the formation of layered $R\bar{3}m$ phase at these charge states. Meanwhile, another set of broad diffraction peaks (solid circles) were consistent with those of rock-salt NiO phase. However, we cannot exclude the formation of copper oxides, which could be embedded in the broad peak area of NiO.

After further charging the electrode to 4.6 V (Figure 4c), the change in phase composition was almost negligible, which remained true for the 2.6 V discharge state as well (Figure 4d), although the root cause for the small variation in the 2θ value of 29−35° was unclear. However, it was noticed that Li_2CO_3 feature was more pronounced at 4.6 V charge. Li_2CO_3 typically exists as surface contaminant, decomposes around 4.3 V upon the first charge, and is permanently eliminated in the later electrochemical processes in other Li-ion cathodes.[35−37] The increase in Li_2CO_3 content at 4.6 V was most likely related to the participation of oxygen and parasitic reactions between electrode and electrolyte in the high voltage region (>4.3 V). On the other hand, most discharge products became amorphous and the original *Immm* structure was not recovered after discharge to 1.5 V. Instead, a Li_2O crystalline phase became more visible.

Hard X-ray Absorption Spectroscopy (XAS). Hard XAS spectra were collected at the Ni and Cu K-edge to investigate the oxidation state change and local environment around Ni and Cu during the electrochemical reaction. According to the X-ray absorption near edge structure (XANES) analysis (Figure 5a), Ni was oxidized from the pristine state to 3.8 V during charge as the Ni edge moved toward higher energy (close to that of $LiNiO_2$ reference) despite the formation of the NiO phase. Upon further delithiation, the Ni edge did not exhibit any obvious change even after charging to 4.6 V, suggesting Ni oxidation completes at 3.8 V. When discharging back to 1.5 V, the original position of the Ni edge was mostly recovered, suggesting most Ni^{2+} reserved at the 1.5 V discharge state. Small difference at 1.5 V discharge from NiO likely resulted from size effect rather than further reduction.[38,39] Presumably, Ni originating from NiO phase that was constantly observed in the ex situ XRD patterns was divalent. In addition, the recovery of Ni^{2+} after discharge suggested the contribution of Ni^{3+} to Ni^{2+} redox upon the insertion of additional lithium into layered oxide during the discharge process.

On the other hand, the shift in Cu edge position was not straightforward to compare as the shape of the spectra changed dramatically. Our data interpretation focuses on the shape of the spectral fine features to guide our analysis on the oxidation state and coordination environment of Cu during the electrochemical reaction. As shown in Figure 5b, the K-edge XANES of Cu in the pristine $Li_2Ni_{0.8}Cu_{0.2}O_2$ exhibited two rising-edge transitions centered around 8984 and 8990 eV, which was in agreement with those of previous reported spectra,[21] corresponding to the electric dipole transitions from the 1*s* state to various *np* final states.[40] When charged to 3.8 V, the two rising edges around 8984, and 8990 eV almost vanished and ended at a more smooth main edge. Such dramatic change in the Cu K-edge XANES, after charging $Li_2Ni_{0.8}Cu_{0.2}O_2$ to 3.8 V, was in agreement with those previously reported by Ruther et al. and could be ascribed to the retained Cu^{2+}.[21] According to the previous electrochemical study on Li_2CuO_2,[27] oxidation of Cu from 2+ to 3+ was possible upon lithium removal. In our case, we did not observe a clear shift in Cu energy edge to support the formation of Cu^{3+} at 3.8 V charge. Similar to the Ni case, no further variation was noticed in the high voltage region. At the 1.5 V discharge state, one rising edge was recovered and shifted to a lower energy around 8981 eV, corresponding to Cu_2O.

The extended X-ray absorption fine structure (EXAFS) directly reflects the local surrounding feature in the short-range structure. The EXAFS of the pristine material (Figure 5c) was

DOI: 10.1021/acs.jpcc.7b01799
J. Phys. Chem. C 2017, 121, 11100−11107

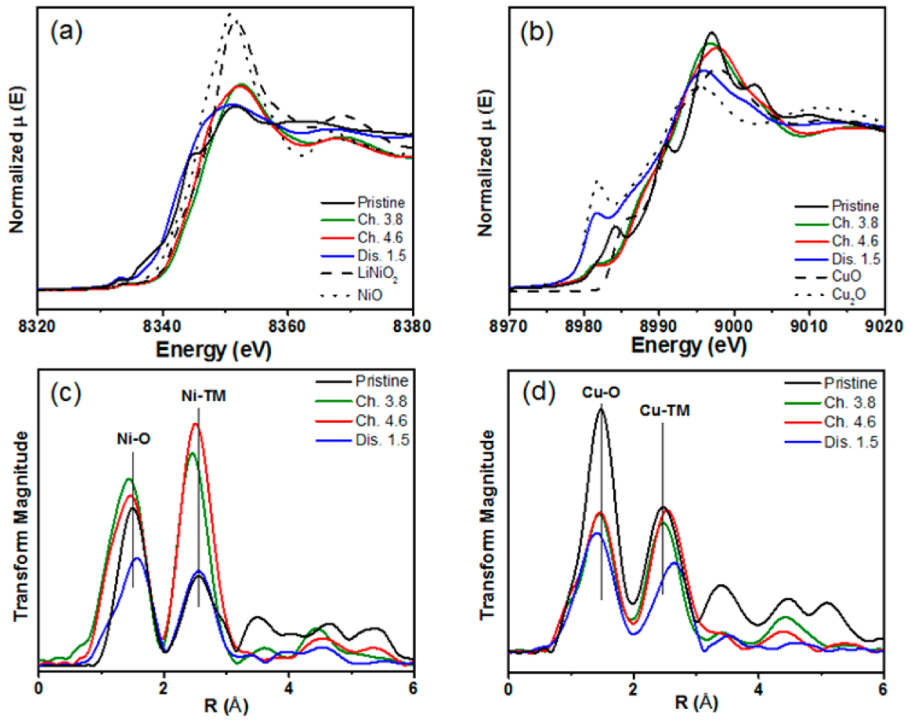

Figure 5. X-ray absorption near edge structure for (a) Ni K-edge, (b) Cu K-edge, and extended X-ray absorption fine structure for (c) Ni K-edge, and (d) Cu K-edge in $Li_2Ni_{0.8}Cu_{0.2}O_2$.

featured by three peaks between 1 and 4 Å, representing the TM−O on the first shell (~1.5 Å, apparent), TM−TM in edge-shared coordination on the second shell (~2.4 Å, apparent), and direct TM−TM scattering in the neighboring plane (~3.3 Å, apparent), respectively.[41] Overall, the significant decrease in the amplitude of the TM−TM peak above 3 Å during the charge−discharge process suggested phase mixture and/or disorder in the cycled electrodes. In the EXAFS of Ni, the distance of Ni−O shell and Ni−TM shell decreased during the charge process due to the Ni oxidation, which was consistent with the XANES results. Another significant change was the amplitude of Ni−TM on the second shell around 2.4 Å from pristine to charged states. In principle, the ratio of Ni−O peak to Ni−TM peak for *Immm* Li_2NiO_2 is 2, while, the ratio is 1 for layered $LiNiO_2$.[9] The significant change in the ratio of Ni−O to Ni-TM at charge states seemed consistent with the transition from square planar coordinated [NiO_4] unit in *Immm* structure to octahedral [NiO_6] coordination in layered $R\bar{3}m$ structure. Afterward, a pronounced increase in Ni−O distance was consistent with Ni reduction at 1.5 V discharge, and significant decrease in the amplitude of Ni−O and Ni−TM peaks was due to the amorphous or nanocrystalline feature after the first discharge.

In the EXAFS of Cu (Figure 5d), the Cu−O shell was maintained at consistent positions during charge; further discharging to 1.5 V led to a shorter Cu−O and longer Cu−TM distance that were associated with the formation of Cu_2O. In addition, the most pronounced feature was a significant drop in the intensity of Cu−O shell in the cycled electrodes compared to that in the pristine electrode. Similar to that of Ni, the ratio of Cu−O to Cu−TM approximately changed from about 2 to 1 during charge, which was an evidence of Cu local symmetry or coordination change. More in-depth analysis of EXAFS in comparison with reference compounds would be useful for the quantitative assessment of TM−O and TM−TM distances, though some reference (e.g., Ni^{4+}) might be obtained by electrochemical or chemical delithiation method. Given both XANES and EXAFS suggested no major change in Ni and Cu edge positions above 3.8 V, the charge compensation in the high voltage region was likely contributed by the participation of oxygen, thus differential electrochemical mass spectrometry (DEMS) was conducted to study the oxygen reactivity.

Differential Electrochemical Mass Spectrometry (DEMS). DEMS was used to characterize gas evolution during the first charge−discharge cycle of a $Li_2Ni_{0.8}Cu_{0.2}O_2$ cathode. The DEMS results were collected under the same electrochemical testing conditions as those shown in Figure 2a. The first cycle voltage profiles from the in situ gas evolution test are similar to those obtained in our regular electrochemical cell tests, with the DEMS cell showing slightly higher over potentials due to a thicker cathode with higher loading. Both the first cycle voltage profiles and in situ gas evolution rates are presented in Figure 6. At the beginning of the charge process, trace amounts (<0.1 nmol/min) of H_2, C_2H_4, and CH_4 were detected but are not shown for clarity. At ~3.7 V, CO_2 began to evolve, increasing in rate with the charge voltage. The CO_2 detected could originate from side reactions with the electrolyte, surface contaminants, or from excited O release from the oxide electrode.[42,43] Beginning at ~4.0 V, there was a burst of O_2 evolution not explained by electrolyte oxidation, suggesting that lattice oxygen ions were directly involved in the redox reaction.[9,21]

The gas evolution measurement provides useful insights into the understanding of anionic oxygen redox during charge, especially in the high voltage region. As discussed above, Ni oxidation was the dominant process up to 3.8 V, followed by almost no detectable change in the oxidation state of Cu and Ni. Therefore, the additional capacity at >3.8 V must involve the participation of electrons removed from the lattice oxygen anions. In-situ gas evolution analysis and material properties are

DOI: 10.1021/acs.jpcc.7b01799
J. Phys. Chem. C 2017, 121, 11100−11107

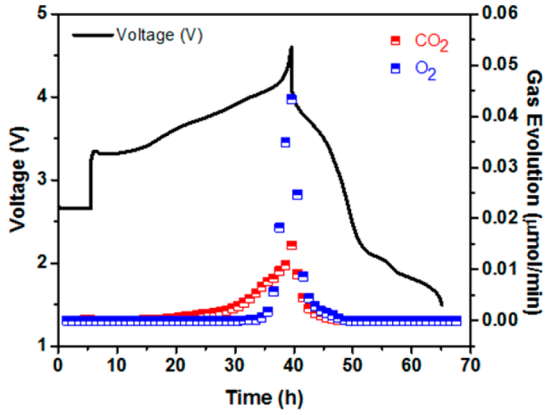

Figure 6. Differential electrochemical mass spectrometry of $Li_2Ni_{0.8}Cu_{0.2}O_2$ during the first cycle (12 mA/g, 4.6–1.5 V).

presented in Table 1. An amount of 26.2 mg of $Li_2Ni_{0.8}Cu_{0.2}O_2$ active material (equivalent to 248 μmol) was used in the in situ

Table 1. In Situ Gas Evolution Analysis and the First Cycle Charge Capacity of $Li_2Ni_{0.8}Cu_{0.2}O_2$

cathode material	$Li_2Ni_{0.8}Cu_{0.2}O_2$
molecular weight (g/mol)	105
Theoretical capacity (mAh/g)	508
charge capacity (mAh/g, OCV −3.8 V)[a]	273
Charge capacity (mAh/g, 3.8–4.0 V)[b]	76
Charge capacity (mAh/g, 4.0–4.6 V)[c]	88
active material weight (mg)	26.2
active material (μmol)	248
evolved O_2 (μmol)	9.0
evolved CO_2 (μmol)	6.6

[a]Charge stage during which Ni and Cu redox is active and minor gas evolution occurs. [b]Charge stage during which no Ni or Cu redox is active, but O_2 evolution has not commenced. [c]Charge stage during which O_2 and CO_2 evolution are active.

gas measurement cell. The evolved gas was composed of 6.6 μmol CO_2 and 9.0 μmol O_2. If we assume that O_2 evolution originated solely from the active electrode (rather than electrolyte decomposition), 3.6% of the oxygen in the $Li_2Ni_{0.8}Cu_{0.2}O_2$ lattice was evolved as O_2. The total capacity corresponding to this evolved O_2 has an upper bound of 37.0 mAh/g, taking a maximum of a 4 electron process for oxidation of the lattice oxygen anions, and assuming that the electrons are fully contributed by the $Li_2Ni_{0.8}Cu_{0.2}O_2$ cathode.

From our electrochemical study, $Li_2Ni_{0.8}Cu_{0.2}O_2$ achieved a charge capacity of ~440 mAh/g and a discharge capacity of ~360 mAh/g in its first cycle, suggesting that the charge capacity of 164 mAh/g above 3.8 V is not completely irreversible. Before O_2 evolution, from 3.8 to 4.0 V (accounting for 76 mAh/g), there is only 1.0 μmol CO_2 detected. Although the exact mechanism of CO_2 evolution is unknown, if we take a rather generous estimate of 8 e^-/CO_2, CO_2 evolution in this range would only account for ~8 mAh/g of the 76 mAh/g capacity. We posit thus that the majority of the charge in the 3.8–4.0 V range is compensated by lattice oxygen. However, above 4.0 V (accounting for 88 mAh/g), the oxygen lattice is unstable and 9.0 μmol O_2 are irreversibly lost from the oxide in addition to a further 5.6 umol CO_2. The irreversible O_2 evolution in this regime only accounts for a maximum of 37 mAh/g and we attribute the remaining 51 mAh/g capacity to a combination of CO_2 evolution and other high voltage parasitic reactions that likely result in nonvolatile products. This seems consistent with our XRD results, which showed an abnormal increase in the amount of Li_2CO_3 after charging at 4.6 V, because its decomposition around 4.3 V during charge is typically observed.

CONCLUSION

We reported the synthesis of $Li_2Ni_{1-x}Cu_xO_2$ solid solutions via a solid-state method. Our electrochemical studies clearly showed the effect of Cu incorporation on the electrochemical performance. The improvement in the overall capacity, particularly during charge, was attributed to the high purity of the final *Immm* type phase. Cu substitution helped stabilize the *Immm* structure, however, such stabilization effect upon delithiation was not as effective as that for synthesis. During the electrochemical process, the materials experienced a series of phase transformation at <3.8 V and Cu incorporation showed a profound influence on the phase transformation route, as evidenced by the variation in voltage plateau with composition. The phase transformation was further confirmed by changes in crystal structure, local symmetry, and coordination in our ex situ XRD and XAS results. Our DEMS measurements showed evolution of CO_2 and O_2 gas on charge in the voltage region of >3.7 V. Our gas evolution results suggested the participation of lattice oxygen in the redox reaction between 3.8–4.0 V, as well as irreversible electrolyte and/or electrode degradation leading to CO_2 evolution above 4 V. The underlying reactions associated with gas evolution are detrimental to the overall electrochemical performance. For future optimization, the key is to suppress or eliminate such undesired phase transformation and accompanying gas evolution. It would be extremely helpful to examine the variation of phase transformation, gas evolution and electrochemical properties with electrolytes. Such evaluation would provide useful insights into in-depth understanding of the contribution of bulk and/or surface properties to these undesired phase transformation and gas evolution behaviors, therefore, proposing effective strategies (e.g., doping, surface coating, and electrolyte additives) to prohibit such unfavorable reactions within the electrode and/or between electrode and electrolyte for further improved electrochemical performance.

ASSOCIATED CONTENT

Supporting Information

The Supporting Information is available free of charge on the ACS Publications website at DOI: 10.1021/acs.jpcc.7b01799.

Comparison of the XRD patterns of $Li_{2-z}Ni_{0.8}Cu_{0.2}O_2$ electrodes at various charged and discharged states with those of possible reference compounds (PDF)

AUTHOR INFORMATION

Corresponding Author

*E-mail: weitong@lbl.gov.

ORCID

Bryan D. McCloskey: 0000-0001-6599-2336
Wei Tong: 0000-0002-2878-1297

Notes

The authors declare no competing financial interest.

DOI: 10.1021/acs.jpcc.7b01799
J. Phys. Chem. C 2017, 121, 11100–11107

■ ACKNOWLEDGMENTS

This work was supported by the Assistant Secretary for Energy Efficiency and Renewable Energy, Office of Vehicle Technologies of the U.S. Department of Energy under Contract No. DE-AC02-05CH11231, under the Advanced Battery Materials Research (BMR) Program. S.E.R. gratefully acknowledges support from the Department of Defense (DOD) through the National Defense Science & Engineering Graduate Fellowship (NDSEG) Program. Synchrotron XAS work was carried out at the Stanford Synchrotron Radiation Lightsource, a Directorate of SLAC National Accelerator Laboratory and an Office of Science User Facility operated for the U.S. Department of Energy Office of Science by Stanford University. Use of the Stanford Synchrotron Radiation Lightsource, SLAC National Accelerator Laboratory, is supported by the U.S. Department of Energy, Office of Science, Office of Basic Energy Sciences under Contract No. DE-AC02-76SF00515.

■ REFERENCES

(1) Etacheri, V.; Marom, R.; Elazari, R.; Salitra, G.; Aurbach, D. Challenges in the Development of Advanced Li-Ion Batteries: A Review. *Energy Environ. Sci.* **2011**, *4*, 3243−3262.

(2) Meng, Y. S.; Arroyo-de Dompablo, M. E. First Principles Computational Materials Design for Energy Storage Materials in Lithium Ion Batteries. *Energy Environ. Sci.* **2009**, *2*, 589−609.

(3) Goodenough, J. B.; Park, K.-S. The Li-Ion Rechargeable Battery: A Perspective. *J. Am. Chem. Soc.* **2013**, *135*, 1167−1176.

(4) Whittingham, M. S. Ultimate Limits to Intercalation Reactions for Lithium Batteries. *Chem. Rev.* **2014**, *114*, 11414−11443.

(5) Xu, J.; Lin, F.; Doeff, M. M.; Tong, W. A Review of Ni-Based Layered Oxides for Rechargeable Li-Ion Batteries. *J. Mater. Chem. A* **2017**, *5*, 874−901.

(6) Dahn, J. R.; von Sacken, U.; Michal, C. A. Structure and Electrochemistry of $Li_{1\pm y}NiO_2$ and a New Li_2NiO_2 Phase with the Ni $(OH)_2$ Structure. *Solid State Ionics* **1990**, *44*, 87−97.

(7) Kang, K.; Chen, C. H.; Hwang, B. J.; Ceder, G. Synthesis, Electrochemical Properties, and Phase Stability of Li_2NiO_2 with the Immm Structure. *Chem. Mater.* **2004**, *16*, 2685−2690.

(8) Lee, H.; Chang, S.-K.; Goh, E.-Y.; Jeong, J.-Y.; Lee, J. H.; Kim, H.-J.; Cho, J.-J.; Hong, S.-T. Li_2NiO_2 as a Novel Cathode Additive for Overdischarge Protection of Li-Ion Batteries. *Chem. Mater.* **2008**, *20*, 5−7.

(9) Back, C. K.; Yin, R.-Z.; Shin, S.-J.; Lee, Y.-S.; Choi, W.; Kim, Y.-S. Electrochemical Properties and Gas Evolution Behavior of Over-lithiated Li_2NiO_2 as Cathode Active Mass for Rechargeable Li Ion Batteries. *J. Electrochem. Soc.* **2012**, *159*, A887−A893.

(10) Park, H.; Yoon, T.; Kim, Y.-U.; Ryu, J. H.; Oh, S. M. Li_2NiO_2 as a Sacrificing Positive Additive for Lithium-Ion Batteries. *Electrochim. Acta* **2013**, *108*, 591−595.

(11) Davidson, I.; Greedan, J. E.; von Sacken, U.; Michal, C. A.; Dahn, J. R. Structure of 1T-Li_2NiO_2 from Powder Neutron Diffraction. *Solid State Ionics* **1991**, *46*, 243−247.

(12) Rieck, H.; Hoppe, R. Ein Neues Oxoniccolat: Li_2NiO_2. *Z. Anorg. Allg. Chem.* **1972**, *392*, 193−196.

(13) Kang, K.; Morgan, D.; Ceder, G. First Principles Study of Li Diffusion in I-Li_2NiO_2 Structure. *Phys. Rev. B: Condens. Matter Mater. Phys.* **2009**, *79*, 014305.

(14) Prakash, A. S.; Larcher, D.; Morcrette, M.; Hegde, M. S.; Leriche, J. B.; Masquelier, C. Synthesis, Phase Stability, and Electrochemically Driven Transformations in the $LiCuO_2$−Li_2CuO_2 System. *Chem. Mater.* **2005**, *17*, 4406−4415.

(15) Berger, R.; Önnerud, P.; Laligant, Y.; Le Bail, A. The Structure of $Li_3Cu_2O_4$, a Compound with Formal Mixed Valence. *J. Alloys Compd.* **1993**, *190*, 295−299.

(16) Berger, R.; Tergenius, L.-E. Room Temperature Synthesis and Structural Characterization of Monoclinic $LiCuO_2$ by X-Ray and Neutron Diffraction. *J. Alloys Compd.* **1994**, *203*, 203−207.

(17) Currie, D. B.; Weller, M. T. Structure of the Mixed-Valence Lithium Cuprate $Li_3Cu_2O_4$ by Powder Neutron Diffraction. *J. Mater. Chem.* **1993**, *3*, 229−232.

(18) Imanishi, N.; Shizuka, K.; Ikenishi, T.; Matsumura, T.; Hirano, A.; Takeda, Y. Preparation and Electrochemical Properties of a Li_2CuO_2-Li_2NiO_2 Solid Solution as a Lithium-Intercalation Electrode. *Solid State Ionics* **2006**, *177*, 1341−1346.

(19) Love, C. T.; Johannes, M. D.; Stux, A. M.; Swider-Lyons, K. Characterization and Electrochemical Properties of $Li_2Cu_{0.5}Ni_{0.4}M_{0.1}O_2$ Lithium-Ion Battery Cathodes. *ECS Trans* **2008**, *16*, 27−35.

(20) Setiawati, E.; Hayashi, M.; Tsuda, M.; Hayashi, K.; Kobayashi, R. Structural Changes and Electrochemical Properties of $Li_2Cu_{1-x}M_xO_2$ for Lithium Secondary Batteries. *Solid State Ionics* **2014**, *262*, 115−119.

(21) Ruther, R. E.; Zhou, H.; Dhital, C.; Saravanan, K.; Kercher, A. K.; Chen, G.; Huq, A.; Delnick, F. M.; Nanda, J. Synthesis, Structure, and Electrochemical Performance of High Capacity $Li_2Cu_{0.5}Ni_{0.5}O_2$ Cathodes. *Chem. Mater.* **2015**, *27*, 6746−6754.

(22) Hoffmann, R.; Hoppe, R.; Schäfer, W. Neutronenbeugung an Li_2CuO_2. *Z. Anorg. Allg. Chem.* **1989**, *578*, 18−26.

(23) Sapiña, F.; Rodríguez-Carvajal, J.; Sanchis, M. J.; Ibáñez, R.; Beltrán, A.; Beltrán, D. Crystal and Magnetic Structure of Li_2CuO_2. *Solid State Commun.* **1990**, *74*, 779−784.

(24) You, S.; Li, Z.; Yang, L.; Dong, C.; Chen, L.; Jin, C.; Hu, J.; Shen, G.; Mao, H. High Pressure Induced Coordination Evolution in Chain Compound Li_2CuO_2. *J. Solid State Chem.* **2009**, *182*, 3085−3090.

(25) Arachi, Y.; Nakata, Y.; Hinoshita, K.; Setsu, T. Changes in Electronic Structure of $Li_{2-x}CuO_2$. *J. Power Sources* **2011**, *196*, 6939−6942.

(26) Patat, S.; Blunt, D. P.; Chippindale, A. M.; Dickens, P. G. The Thermochemistry of LiCuO, Li_2CuO_2 and $LiCu_2O_2$. *Solid State Ionics* **1991**, *46*, 325−329.

(27) Arai, H.; Okada, S.; Sakurai, Y.; Yamaki, J.-i. Electrochemical and Structural Study of Li_2CuO_2, $LiCuO_2$ and $NaCuO_2$. *Solid State Ionics* **1998**, *106*, 45−53.

(28) Raekelboom, E. A.; Hector, A. L.; Weller, M. T.; Owen, J. R. Electrochemical Properties and Structures of the Mixed-Valence Lithium Cuprates $Li_3Cu_2O_4$ and $Li_2NaCu_2O_4$. *J. Power Sources* **2001**, *97*−*98*, 465−468.

(29) Vitins, G.; Raekelboom, E. A.; Weller, M. T.; Owen, J. R. Li_2CuO_2 as an Additive for Capacity Enhancement of Lithium Ion Cells. *J. Power Sources* **2003**, *119*−*121*, 938−942.

(30) Love, C. T.; Dmowski, W.; Johannes, M. D.; Swider-Lyons, K. E. Structural Originations of Irreversible Capacity Loss from Highly Lithiated Copper Oxides. *J. Solid State Chem.* **2011**, *184*, 2412−2419.

(31) Arachi, Y.; Setsu, T.; Ide, T.; Hinoshita, K.; Nakata, Y. Reversible Electrochemical Reaction of CuO with Li in the $LiCuO_2$ System. *Solid State Ionics* **2012**, *225*, 611−614.

(32) Nakamura, K.; Moriga, T.; Sumi, A.; Kashu, Y.; Michihiro, Y.; Nakabayashi, I.; Kanashiro, T. Nmr Study on the Li^+ Ion Diffusion in $LiCuO_2$ with Layered Structure. *Solid State Ionics* **2005**, *176*, 837−840.

(33) Nakamura, K.; Kawai, K.; Yamada, K.; Michihiro, Y.; Moriga, T.; Nakabayashi, I.; Kanashiro, T. Li+ Ionic Diffusion in Li−Cu−O Compounds. *Solid State Ionics* **2006**, *177*, 2775−2778.

(34) McCloskey, B. D.; Bethune, D. S.; Shelby, R. M.; Girishkumar, G.; Luntz, A. C. Solvents' Critical Role in Nonaqueous Lithium−Oxygen Battery Electrochemistry. *J. Phys. Chem. Lett.* **2011**, *2*, 1161−1166.

(35) Han, S.; Xia, Y.; Wei, Z.; Qiu, B.; Pan, L.; Gu, Q.; Liu, Z.; Guo, Z. A Comparative Study on the Oxidation State of Lattice Oxygen among $Li_{1.14}Ni_{0.136}Co_{0.136}Mn_{0.544}O_2$, Li_2MnO_3, $LiNi_{0.5}Co_{0.2}Mn_{0.3}O_2$ and $LiCoO_2$ for the Initial Charge-Discharge. *J. Mater. Chem. A* **2015**, *3*, 11930−11939.

(36) Wang, R.; Yu, X.; Bai, J.; Li, H.; Huang, X.; Chen, L.; Yang, X. Electrochemical Decomposition of Li_2CO_3 in NiO−Li_2CO_3 Nanocomposite Thin Film and Powder Electrodes. *J. Power Sources* **2012**, *218*, 113−118.

DOI: 10.1021/acs.jpcc.7b01799
J. Phys. Chem. C 2017, 121, 11100−11107

(37) Xu, J.; Lin, F.; Nordlund, D.; Crumlin, E. J.; Wang, F.; Bai, J.; Doeff, M. M.; Tong, W. Elucidation of the Surface Characteristics and Electrochemistry of High-Performance $LiNiO_2$. *Chem. Commun.* **2016**, *52*, 4239−4242.
(38) Dai, Y.; Gorey, T. J.; Anderson, S. L.; Lee, S.; Lee, S.; Seifert, S.; Winans, R. E. Inherent Size Effects on Xanes of Nanometer Metal Clusters: Size-Selected Platinum Clusters on Silica. *J. Phys. Chem. C* **2017**, *121*, 361−374.
(39) Boesenberg, U.; Marcus, M. A.; Shukla, A. K.; Yi, T.; McDermott, E.; Teh, P. F.; Srinivasan, M.; Moewes, A.; Cabana, J. Asymmetric Pathways in the Electrochemical Conversion Reaction of NiO as Battery Electrode with High Storage Capacity. *Sci. Rep.* **2015**, *4*, 7133.
(40) Alp, E. E.; Shenoy, G. K.; Hinks, D. G.; Ii, D. W. C.; Soderholm, L.; Schuttler, H. B.; Guo, J.; Ellis, D. E.; Montano, P. A.; Ramanathan, M. Determination of Valence of Cu in Superconducting $La_{2-x}(Sr, Ba)_xCuO_4$. *Phys. Rev. B: Condens. Matter Mater. Phys.* **1987**, *35*, 7199−7202.
(41) Kim, M. G.; Cho, J. Air Stable Al_2O_3-Coated Li_2NiO_2 Cathode Additive as a Surplus Current Consumer in a Li-Ion Cell. *J. Mater. Chem.* **2008**, *18*, 5880−5887.
(42) Wuersig, A.; Scheifele, W.; Novák, P. CO_2 Gas Evolution on Cathode Materials for Lithium-Ion Batteries. *J. Electrochem. Soc.* **2007**, *154*, A449−A454.
(43) Onuki, M.; Kinoshita, S.; Sakata, Y.; Yanagidate, M.; Otake, Y.; Ue, M.; Deguchi, M. Identification of the Source of Evolved Gas in Li-Ion Batteries Using ^{13}C-Labeled Solvents. *J. Electrochem. Soc.* **2008**, *155*, A794−A797.

DOI: 10.1021/acs.jpcc.7b01799
J. Phys. Chem. C 2017, 121, 11100−11107